Quiet time solar illumination effects on the fluxes and characteristic energies of ionospheric outflow.

W.K. Peterson[1], H.L. Collin[2], O.W. Lennartsson[2] and A.W. Yau[3]

[1]Laboratory for Atmospheric and Space Physics, University of Colorado, 1234 Innovation Drive, Boulder, Colorado, 80304 USA

[2]Advanced Technology Center, Lockheed Martin Space Systems Company, Palo Alto, California, 94304, USA

[3]University of Calgary, Department of Physics and Astronomy, Institute for Space Research, 2500 University Dr NW, Calgary Alberta T2N1N4 Canada

Revised March 17, 2006.

Abstract

We report on the characteristic energy, intensity, and flow rate of escaping ionospheric ions as a function of solar illumination. The data presented here were acquired with the Toroidal Ion Mass-Angle Spectrograph (TIMAS) instrument on the Polar satellite at altitudes of 6,000 to 9,000 km, during solar minimum. To obtain uniform coverage under various solar illumination conditions, data were restricted to geomagnetically quiet intervals when the Dst index was above -50 nT. We explicitly report data for four magnetic local time ranges. Our investigation confirms many of the characteristics of ion outflows deduced from earlier episodic studies, and identifies an anticorrelation in the dependence of beam and conic fluxes on solar illumination, which we attribute to variations in the altitude at which auroral acceleration processes occur. We find that the cusp is an important but not dominant source of ionospheric plasma for the magnetosphere. We conclude that significantly different plasma energization and/or transport mechanisms are dominant in the cusp and the midnight sectors. In addition, we conclude that variations in the solar EUV and geomagnetic energy inputs into the ionosphere, rather than the longer time scale seasonal and annual variations in solar illumination, determine the global rates of H^+ and O^+ outflow. The data presented here provide comprehensive and realistic boundary conditions for large-scale magnetospheric models during non-storm times.

Introduction

The ionosphere is an important and sometimes dominant source of plasma in the Earth's magnetosphere. The energization and transport processes that extract, energize, and transport cold ionospheric ions such as H^+, He^+, O^+, and NO_2^+ into the cool polar wind, the warm plasmasphere, the hot plasma sheet, and energetic ring current are many and diverse. Variable mass composition in these regions has been shown or suggested to influence the dayside

reconnection rate [e.g. Chen and Moore, 2004], ULF pulsations and ring current energization processes [e.g. Elkington *et al.* 2003 and Fraser *et al.* 2005], and the onset and frequency of substorms [e.g. Cully *et al.* 2003b and Kistler *et al.* 2005]. Understanding these processes is the central theme of magnetospheric research.

The upflowing fluxes associated with the ionospheric sources of magnetospheric plasma have been empirically characterized over the years using data obtained from increasingly sophisticated instruments. Reviews of this work have been given by Johnson [1983], Shelley and Collin [1991], Yau and André [1997], Moore *et al.* [1999a], and others. Recent results from the Polar, FAST, and Akebono satellites have extended our understanding of both the fluxes [Peterson *et al.* 2001, Seki *et al.* 2003, Cully *et al.* 2003a, and Huddleston *et al.* 2005] and the characteristic energies [Lennartsson *et al.* 2004, Abe *et al.* 2004, and Andersson *et al.* 2005] of these ionospheric sources. Progress in identifying and understanding the dominant physical mechanisms responsible for energizing and transporting ionospheric plasma to the magnetosphere has been less rapid. See, for example, Chappell *et al.* [1987], André and Yau [1997], Hultqvist *et al.* [1999], and Strangeway *et al.* [2005].

Modelers have begun to explore ionospheric energization and transport processes [e.g. Winglee 2003, Ashour-Abdalla *et al.* 2000, and Cully *et al.* 2003b]. Limited progress has been made because it is challenging to include ionospheric plasmas in large-scale magnetospheric models. The challenge to modelers is to relate model-derived quantities such as solar illumination and Poynting flux and data-derived quantities such as fluxes and characteristic energies to physical processes responsible for ion outflow and energization. Modelers also need more observational data on characteristic energies and magnetic local time distributions of outflows than is currently available to constrain their models..

Reports by Yau *et al.* [1985], Newell *et al.* [1996], Abe *et al.* [2004], and others have demonstrated the role of solar illumination in modulating ionospheric energization and transport processes. The variation in solar illumination available in these reports was limited by orbital and data processing constraints to seasonal or sunlight/not sunlight conditions. Information about the variation of ion outflow intensity and characteristic energy as a function of solar illumination (i.e. solar zenith angle) is required to quantitatively evaluate the importance of solar illumination in energizing and transporting magnetospheric plasmas.

This report examines the intensity and characteristic energy of ion outflows during solar and geomagnetically quiet times as a function of solar illumination observed by the Toroidal Ion Mass-Angle Spectrograph (TIMAS) instrument on the Polar satellite during perigee passes. We explicitly report data for four magnetic local time ranges. Data from Polar satellite apogee passes was not included because the data base would be temporally aliased by magnetospheric events occurring on time scales less than the long (~12 hour) time scales required to obtain data from one apogee pass. To obtain uniform coverage under various solar illumination conditions, data were restricted to geomagnetically quiet intervals when the Dst index was above -50 nT.

Observations

Figure 1 presents the average number and energy fluxes of H^+, O^+, and He^+, observed from March 18, 1996 through December 8, 1998 by the TIMAS instrument during Polar perigee passes. The data were obtained over the energy range 15 eV < E/q < 33 keV and have been normalized to an altitude of 300 km and are presented in units of ions m^{-2} s^{-1} and keV m^{-2} s^{-1}, respectively. The data and the methods used to accumulate and display them have been described by Peterson *et al.* [2001] and Lennartsson *et al.* [2004]. Explicitly, the number flux at a particular invariant latitude, magnetic local time, and reference altitude is the integral of the measured differential number flux over energy and solid angle, normalized to the reference altitude. Consistent with Yau et al.,[1988], Collin et al. [1988], Peterson et al. [2001], and Lennartsson et al. [2004], a correction has been made for energetic ions precipitating into the ionosphere (i.e. absorbed and not reflected). This component has a net downflow, which causes the outflow to be underestimated. The correction was made by calculating the net outflow rate that would have corresponded to a nominal loss cone filled with the observed downward field aligned ion flux. Correcting for the precipitation downflow resulted in a significant but not overwhelming increase in the total net outflow rate in the H^+ but little change in the other species. The correction is largest equatorward of the normal auroral zone.

Because geomagnetic storms were infrequent during the 1996-1998 interval of interest, and the Polar orbit completed only two full cycles of invariant latitude/magnetic local time coverage per year, we have excluded storm time intervals (when the hourly average Dst index is above minus 50 nT). The geomagnetic activity restriction reduces temporal aliasing introduced by intense storm-time fluxes. Because the Polar satellite crosses the auroral zones at perigee in ~15 minutes, the restriction to data acquired at perigee reduces temporal aliasing. The data in Figure 1 were obtained during solar and geomagnetically quiet times. The average value of the $F_{10.7}$ index was 92. The average value of the Dst index was -11; the average value of the K_P index and the A_E index were 2- and 221, respectively.

The number fluxes presented in Figure 1 differ in appearance from plots of the same data presented in Peterson *et al.* [2001, Plate 1], and Lennartsson *et al.* [2004, Figure 1]. These differences arise because the display and selection criteria used were different. The resolution in invariant latitude and magnetic local time used throughout this paper is 5° and 1.5 hours respectively, which is coarser than the resolution in previous reports, in order to retain adequate sampling in the subdivided data sets described below. The data presented in Peterson *et al.* [2001] were displayed for five 6-month intervals. The data here are averaged over 34-months, including the five 6-month intervals in Peterson *et al.* The data presented in Lennartsson *et al.* [2004], Figure 1, were accumulated by excluding earthward (negative) H^+ flows and equating each earthward flow density sample with a zero-flow sample, in order to simplify apogee/perigee comparisons of H^+ flows in the cusp. In the perigee data presented here, we verified that the net flux associated with precipitating and reflecting cusp H^+ is negligible. The black pixels in Figure 1 indicate regions of net downward flux. The downward fluxes observed are less than ~10^{10} m^{-2} s^{-1} over limited spatial regions for H^+ and O^+ and less than 10^9 m^{-2} s^{-1} for He^+. The regions of net downward fluxes therefore do not dominate the calculation of total outflowing flux.

Table 1 presents the net hemispheric ion outflow rate and average ion energy for the three ion species, derived from the data in Figure 1. The outflow rate is given in the units of 10^{24} ions s^{-1}, and the energy unit is keV. The methods used to obtain these averages for H^+ and O^+ are described in Lennartsson *et al.* [2004]. In brief, the net ion outflow rate is the sum over all invariant-latitude-MLT bins (5 deg by 1.5 h) above a given latitude of the averaged (and normalized) net outward flux within each bin, multiplied by the bin surface area at 300 km altitude. The ion energy is "flow averaged" in the sense that it is derived by integrating the net outward energy flux the same way and dividing it by the net ion outflow rate. Data for three low-latitude boundaries are reported. Integral fluxes obtained from higher resolution bins were not significantly different. The literature sometimes uses the term "fluence" to mean the same net ion outflow rate (e.g. Peterson et al. [2001]).

Table 1: Net hemispheric ion outflow rates and average ion energies

Invariant	Net Outflow Rate (10^{24} ions s^{-1})			Energy (keV)		
Latitude	H^+	O^+	He^+	H^+ *	O^+	He^+ *
>55°	1.7	2.4	0.18	1.9	0.34	1.9
>60°	1.8	2.4	0.19	1.6	0.32	1.8
>65°	1.5	1.9	0.16	1.3	0.3	0.75

*As discussed in text, the energies in this table for H^+ and He^+ are significantly biased upward.

Lennartsson *et al.* [2004] described the major instrumental effects that may bias the determination of the net outflow rate and energy. Two factors are especially important in determining the average energy: computing errors introduced in the process of correcting for the effects of precipitating and trapped magnetospheric ions, which are due in part to spatial and temporal variations of the magnetospheric populations, and the exclusion of escaping thermal plasma from below the TIMAS energy range.

Lennartsson [2004] showed that the net outflow rate and energy values obtained depend on the lower limit of invariant latitude in the analysis. Values for three lower invariant latitude limits are shown in Table 1. As discussed below we have extended the analyses of Lennartsson et al. [2004] and Peterson *et al.* [2001] to include outflow rates and characteristic energies for upflowing distributions with well-defined “beam” or “conic” distributions and for magnetic local time quadrants. A detailed analysis of flow rates and energies derived from these subsets of the data presented in Figure 1 showed that the net outflow above 60^o was nearly equal to that above 55^o, while the characteristic energies using data acquired above 55^o were in certain cases significantly higher than those derived from data acquired above 60^o only. The values of outflow rate and average or “characteristic” energy reported in the rest of this paper are averages above 60^o invariant latitude.

The energies presented in Table 1 are the average energies over the full TIMAS energy range ($0.015 < E/q < 33$ keV/q). With the exception of He^+, the outflow rates and average energies reported in Table 1 are consistent with those presented by Peterson *et al.* [2001] and Lennartsson *et al.* [2004]. As discussed in the paragraphs below, the correction made to account for the apparent downward flux associated with “loss cone” distributions observed in regions of precipitating magnetospheric ions introduces uncertainties into the calculations of net outflow

rates and characteristic energies. We attribute the significantly lower He^+ flow rates reported here in comparison with those reported by Peterson *et al.* [2001] (~0.9 x 10^{24} ions/s) to the improved corrections for the net downward flux of precipitating magnetospheric ions. Likewise, we conclude that the average energies for H^+ and He^+ reported in Table 1 are significantly biased upward.

The uncertainty in the energy fluxes shown in Figure 1 and the derived average energies is larger than that in the number fluxes. The characteristic energy of precipitating ions is greater than that of upflowing ions. Thus the errors in energy flux introduced in the process of removing the net downward contribution of precipitating ions are significantly larger than those in upward number flux. Because the loss cone is not sharply defined and its estimated size may be inaccurate, both the number and energy fluxes may be significantly over-estimated in regions of strong precipitating and trapped hot ion distributions. The errors are especially large in the case of He^+, because most of the He^+ data were acquired with reduced energy and angular resolution compared to the other species due to telemetry rate restrictions.

The uncertainty introduced by the correction for precipitating ions is clearly evident in the He^+ energy fluxes between 60° and 65° invariant latitude (the next to outer ring) on the dusk side in Figure 1. We expect a net upward flux of low energy He^+ below the 15 eV TIMAS energy threshold in this region associated with plasmaspheric refilling, as well as a precipitating flux of energetic He^+ from the plasma sheet. Because of the lack of strong outflow of both H^+ and O^+ in this invariant latitude/local time region, we do not expect significant fluxes of upward ~keV He^+ from auroral acceleration processes. These facts, and the fact that the average He^+ energy above 65° invariant reported in Table 1 is significantly smaller than that in this region (55°-60° invariant), suggest that the average energy of He^+ of 1.8 keV above 60° in Table 1 is biased upward by the imprecise numerical methods. Based on a similar analysis we conclude that the H^+ average energies reported in Table 1 are also biased upward, because of the much higher and often rapidly varying energy density of the precipitating and trapped H^+ populations.

A second source of upward bias to the H^+ and He^+ energies in Table 1 is the exclusion of the contribution of ions below the TIMAS energy-per-charge threshold (15 V, plus the spacecraft potential). Peterson *et al.* [2001], Cully *et al.* [2003a], Lennartsson *et al.* [2004] and Andersson *et al.* [2005] have noted that the various reported values for H^+ and O^+ outflow rates are fairly consistent if there is modest (i.e. ~ 20 eV) acceleration of the thermal plasma between the Akebono and Polar apogees, and if one notes that the thermal plasma observations from Akebono have been corrected for spacecraft potential but exclude ions with energies greater than 70 eV. The data in Table 2 summarize the various reports of the global average ion outflow rates, the altitudes at and energy ranges over which data were accumulated, and the effective O^+ escape energy at each altitude. Based on the Polar Apogee data presented in Table 2 we estimate that the flow rates in Table 1 represent more than 20% of the total, including thermal, escaping H^+ and O^+ fluxes. Table 2 also shows that, at 8,000 km, a larger fraction of the thermal O^+ than H^+ observed on Akebono has been energized into the TIMAS energy range.

Table 2 Average hemispheric ion outflow rates, and measurement altitudes and energy ranges

Satellite	Altitude (km)	Energy Range (keV)	O^+ Escape Energy (keV)	Net Outflow Rate (10^{24} ions/s)		
				H^+	O^+	He^+
Polar (Apogee)[1]	50,000	0.015 - 33	0.001	10	15	-
DE – 1[2,3]	20,000	0.010 - 17	0.002	10	7	0.8
Polar (Perigee)[1,4]	8000	0.015 - 33	0.005	3	3	0.2
Akebono[5]	9000	0.000 – 0.07	0.004	20	2	-
FAST[6]	3000	0.003 - 12	0.007	-	2	-

[1]Lennartsson *et al.* [2004], [2]Yau *et al.* [1986], [3]Collin *et al.* [1988], [4]Peterson *et al.* [2001], [5]Cully *et al.* [2003a], [6]Andersson *et al.* [2005]

It is not physically realistic to characterize the upward flux of ions at Polar perigee altitude by a single energy. Andersson *et al.* [2005] have shown that at altitudes of ~3,000 km the characteristic O^+ energy varies significantly as a function of magnetic local time. Other observations and theoretical analyses indicate that the dominant thermal ion energization processes are not the same in different local time sectors; see for example the reviews of Yau and André [1997] and André and Yau [1997]. It is therefore necessary to examine the characteristic energies as a function of local time, and to differentiate between different ion acceleration and energization mechanisms using available observation data. An often-used approach for doing so is to characterize the ion angular distributions as 'beam', 'conic', or 'upflowing ion' distributions. At Polar altitudes, such distributions are indicative of energization processes acting mostly at altitudes well removed from the ionosphere.

An ion beam is an ion distribution that is peaked along the upward direction of the magnetic field line, and an ion conic is one that is peaked at an angle to the field. Ion beams and conics are not always uniquely defined, however. Details of the definitions differ between instruments and data sets. Trapped distributions created by mirroring down flowing ions are difficult to differentiate from conic distributions peaked at or near 90°. In addition, the energy and angular resolutions of ion detectors are often broad compared to the energy width of ion beams and the angular width of ion conics. The TIMAS instrument has ~20^o angular resolution and energy resolution ($\Delta E/E$) varying from ~0.7 at the lowest energy to ~0.08 above ~1 keV. As noted above, the energy and angular resolution of the He^+ data was further reduced because of telemetry rate constraints.

Following the procedure outlined in Collin *et al.* [1998], we have separated the TIMAS data presented in Figure 1 into three broad energy bands (0.015-0.3, 0.3-4, and 4-33 keV, respectively) and classified the angular distribution in each energy band in terms of three angular distribution types: beam, conic, and upflowing ion (UFI) distributions. We have examined the ion pitch-angle distribution in each energy band in each 12-s measurement interval, to determine the presence of a peak in the distribution in which (1) the full angular width at half maximum is less than 45°, (2) the peak flux is greater than 10^{10} ions/m^2-s-sr, and (3) the peak flux is above the energy-dependent noise threshold. For the southern hemisphere data considered here, ion beams (beam distributions) are defined as having pitch angle peaks in the range of 0° to 30°, and ion conics (conic distributions) in the range of 30° to 75°. Here we define upflowing ion distributions (UFI) as the combination of beams and conics. Thus UFI distributions have peak

pitch angles in the 0° to 75° range. The angular ranges only include pitch angles less than 90°, reflecting the direction of the magnetic field in the southern hemisphere and the exclusion of trapped distributions as well as 90° conic distributions, which are easily confused with trapped particle distributions. We also note that a given 12-s measurement interval is classified as a "beam" or "conic" interval when "beam" or "conic" angular distributions are found in any of the three energy bands. Thus a measurement interval can, at times, be characterized as both a "beam" and "conic" interval. *The definition of "beam", "conic", and "UFI' used here are therefore instrument specific. The reader should note that the automated nature of our determination required the exclusion of ion angular distributions peaking at 90^o from our "conic" and "UFI" distributions.*

Figure 2 displays the net upflowing fluxes for the beam, conic, and UFI angular distribution types in the same format and with the same color codes for the upflowing fluxes as in Figure 1. Conic distributions are created by processes that transfer energy to the ions in a direction perpendicular to the local magnetic field. Beam distributions may be created either by the same processes at much lower altitude or by processes that act primarily in the magnetic field direction. UFI distributions presented here are the large subset of net upward ion fluxes with distinct angular flux peaks that have fluxes greater than 10^{10} ions/m2-s-sr, indicative of distributions significantly affected by acceleration processes well above ionospheric altitudes. Identification of beam, conic and UFI distributions requires existence of a statistically meaningful peak in an ion distribution. Detecting such peaks requires setting a relatively high threshold (10^{10} ions/m2-s-sr) below which distributions are not considered. Thus beam, conic, and UFI events are more intense than distributions that include ion fluxes below the threshold.

We have divided the data presented in Figures 1 and 2 into four magnetic local time (MLT) quadrants: noon, dusk, midnight, and dawn centered at 12, 18, 00, and 06 hours, respectively, and determined the net ion outflow rate and characteristic energy in each quadrant for beams, conics, and UFI distributions. In each MLT quadrant and for each angular distribution type the average energy is derived from the appropriate ratios of energy and number fluxes observed above 60^o invariant latitude. The results of these calculations are presented in Table 3. Column 3 in this Table presents the percentage of net outflow rate of each of the 3 angular distribution types (column 2) for each of the three ion species (column 1). Columns 4-7 present the percentage for each MLT quadrant in each case. The corresponding percentage for "all distributions", which includes all data samples irrespective of their angular distributions, is also presented. Columns 8-11 present the characteristic energies in each case (angular distribution type and MLT quadrant). The beam and conic percentages do not always add up to the UFI percentage due to round off and, in the case of O^+, the small but measurable (~2%) number of intervals, which are identified as both "beam" and "conic". The percentage flux reported in columns 3-6 refers to percentage of each quadrant in each species and angular distribution type. For example, 3.7% (10% × 37%) of H^+ net outflow is associated with ion beams in the noon (12 MLT) quadrant. The sum of percentages over all 4 quadrants may not add up to 100% due to round off. The average UFI energies are the flux-weighted averages of the corresponding beam and conic energies.

As noted above, the determinations of energy flux and characteristic energy are compromised by the approximations made in estimating the size of the loss cone. The largest

errors are introduced in regions of strong precipitating and trapped ion distributions. We have not reported average energies for H^+ and He^+ for all distributions (indicated by * in Table 3) because we concluded that the values derived with this method may not be realistic. If there is an upflowing ion beam or conic, however, the higher flux threshold (10^{10} ions/m2-s-sr) we have set for their identification ensures that the contribution to the net energy flux from the loss cone correction is less important. It is important to note here that, the exclusion of upflowing fluxes below 15 eV and uncertainties introduced by the loss cone correction, lead to the result that the average energies reported in Table 3 are upper limits. The 15 eV TIMAS energy threshold means that the average fluxes reported in Table 3 are lower limits.

Table 3 Outflow rate percentages and characteristic energies by MLT quadrant and angular distribution type

Species	Type	Outflow	Percentage by Quadrant[b]				Energy (keV)[c]			
		Rate %[a]	**12**	**18**	**24**	**06**	**12**	**18**	**24**	**06**
H^+	All distributions	100	29	14	34	22	*	*	*	*
	Beam	37	10	21	43	27	0.34	0.66	1.18	0.34
	Conic	31	25	11	41	23	0.06	0.20	0.18	0.16
	UFI	67	17	16	42	25	0.14	0.49	0.71	0.26
O^+	All distributions	100	37	11	32	20	0.23	0.37	0.43	0.28
	Beam	25	16	25	37	22	0.23	0.56	0.88	0.48
	Conic	58	37	8	32	23	0.11	0.17	0.14	0.13
	UFI	80	31	13	33	23	0.13	0.38	0.39	0.22
He^+	All distributions	100	23	16	40	21	*	*	*	*
	Beam	38	13	21	40	26	0.41	0.80	0.89	0.42
	Conic	18	24	13	42	22	0.22	0.23	0.35	0.18
	UFI	55	17	19	40	25	0.32	0.67	0.70	0.35

(a) The beam and conic percentages may not add up to the UFI percentage due to round-off, and, in the case of O^+, the small but measurable number of intervals that are identified as both "beam" and "conic".
(b) Percentage refers to percentage of each quadrant in each species and angular distribution type. For example, 3.7% (10% × 37%) of H^+ net outflow is associated with ion beams in the noon (12 MLT) quadrant. The sum of percentages over all 4 quadrants may not add up to 100% due to round off.
(c) * indicates significantly biased estimate of characteristic energy (not reported)

Table 3 shows some of the significant impacts solar illumination has on ion energization and transport processes. The largest fraction of outflowing H^+ and He^+ (34% and 40%, respectively) and the second largest fraction of O^+ (32%) in the TIMAS energy range occur in the midnight (24 MLT) quadrant, while the largest fraction of O^+ (37%) occurs in the noon (12 MLT) quadrant. The characteristic energies vary considerably by angular distribution type and MLT quadrant. The characteristic energies of H^+ and He^+ for beams, conics, and UFI are significantly lower than the corresponding energies for all data samples irrespective of their angular distributions. The lowest characteristic energy (~<100 eV) is seen in H^+ and O^+ conics in the noon (12 MLT) quadrant. The highest characteristic energies occur in H^+ beams in the midnight quadrant. Table 3 also shows that a predominant fraction (80%) of the O^+ outflow occurs in the form of UFI distributions indicating the importance of acceleration processes occurring above the ionosphere.

To assess the role of solar illumination on the sources and mechanisms responsible for the variations in fluxes and characteristic energies in the different MLT quadrants, we have examined the data presented above as a function of the solar zenith angle (SZA) at the foot of the magnetic field line passing through the Polar satellite at the time of each 12-s measurement interval. Figure 3 presents the data in Figure 1 sorted by SZA. It shows the net upward number fluxes for H^+, O^+ and He^+ (top three rows) and the number of 12-s samples (bottom row) in each 5° × 1.5 hr invariant latitude-MLT bin, for SZA ranges of 0°-80°, 80°-90°, 90°-100°, and 100°-180°, respectively (from left to right). The average SZA over all sampled MLT and invariant latitude bins in the respective SZA ranges was 64°, 85°, 95° and 115°, respectively. The choice of SZA ranges was made to ensure complete invariant latitude, magnetic local time coverage. As noted below seasonal data sets acquired within ±30 days of solstice or equinox do not have complete coverage. Because of these limitations, we have not considered the orientation of the magnetic dipole which, as discussed in Lennartsson et al. [2004], could also affect outflow on the dayside.

The black areas in the distributions in Figure 3 show extensive regions of downflowing ions at low latitudes. These occur on the dusk sector during periods of sunlight and the dawn sector during periods of darkness. This is not an IMF effect, as the average IMF B_y components sampled in the four SZA ranges were similar and were 0.18, 0.15, 0.22, and 0.19 respectively. Figure 3 clearly shows the decrease of intensity and extent of O^+ in the dayside cusp region with decreasing solar illumination (increasing SZA), and the opposite effect in the He^+. Both effects have been previously reported. See, for example, Yau and Andre [1997] and Collin *et al.* [1988]. Also apparent in both this figure and Figure 5 below is the increasing (decreasing) intensity and extent of H^+ and He^+ (O^+) fluxes on the night side with decreasing solar illumination. These effects have not been reported previously.

The upward number flux distributions in Figure 3 include all data samples irrespective of their angular distributions. Figure 4 presents the corresponding distributions for beam and conic distributions for the same SZA ranges. The UFI distributions are not shown. The most visible features in Figure 4 are the decrease (increase) of the dayside fluxes and extent of O^+ conic (He^+ beam and conic) distributions. Also apparent is the increase in intensity and extent of nightside beam distributions with decreasing solar illumination.

Figure 5 presents the net outflow rates and average characteristic energies derived from the data presented in Figures 3 and 4. These include all data samples irrespective of their angular distributions (i.e. the category of "all distributions" in Table 3) and corresponding rates and energies for beam and conic distributions presented in Figure 4 as well as those for UFI distributions. In Figure 5, diamonds (◊) denote data acquired during quiet intervals (Dst > -50), asterisks (*) denote the full data set that includes both quiet and storm time data, and pluses (+) denote seasonal data sets acquired within ±30 days of the solstice or equinox. Because of the Polar orbit, not all invariant latitude/MLT bins are sampled in a 61-day period. The integral fluxes reported in Figure 5 for the seasonal data sets were made assuming no contribution from the unsampled low invariant-latitude bins in the 06:00 to 07:30 and 18:00 to 19:30 magnetic local time bins. Both the seasonal and full data are presented as a function of the average SZAs observed over the sampled MLT/invariant latitude regions.

The straight lines in Figures 5a and 5b are linear fits to the logarithms of quiet-time outflow rates and characteristic energies, respectively, as a function of solar zenith angle (data denoted by the diamonds (◊). These lines are included only to guide the eye. In spite of the apparently good fits in some cases, there was no physical reason for choosing this function. We note the relatively strong increases in H^+ beam and O^+ UFI characteristic energies with decreasing solar illumination.

As noted above, it is not physically realistic to characterize the ion outflows observed at Polar perigee altitude by a single energy. It is instructive, however, to compare and contrast the dependence of the outflow rates and characteristic energies of the various MLT quadrants with the averages presented in Figure 5. Table 4 summarizes the variation of the outflow rates and characteristic energies with SZA. In this table, the variation in each MLT quadrant with increasing SZA (decreasing solar illumination) is characterized by four symbols: the treble plus ("+++"), single plus ("+"), single minus ("-"), and treble minus ("---") symbols denote strongly positive, weakly positive, weakly negative, and strongly negative dependence, respectively, on SZA (slope of the linear fit of the log outflow rate versus SZA in Figure 4). Here a positive dependence that is similar to or stronger than that for H^+ beams in Figure 4 is identified as "strongly positive". The average characteristic energy (over all SZA ranges) for each angular distribution type and MLT quadrant is reproduced from Table 3. For several MLT quadrants, mass species, and angular distribution types, it was not possible to unambiguously identify the SZA dependence of the flux or characteristic energy. These instances are indicated by asterisks (*) in the table.

Several features stand out in Table 4. Increasing net outflow of all H^+ and O^+ distributions with increasing sunlight (i.e. decreasing solar zenith angle) is seen only in the noon and dawn quadrants. In the dusk and midnight quadrants, the net outflow of all ions increases with decreasing solar illumination, consistent with the results of Collin *et al.* [1998] and others noted in that paper. The characteristic energies for H^+ and O^+ in the midnight quadrant have different behaviors for beams and conics. The characteristic energies of both O^+ beams and conics increase with decreasing solar illumination; the characteristic H^+ beam energy increases, but the characteristic H^+ conic energy decreases with decreasing illumination. In the dawn, noon and dusk quadrants the increase in outflow rates of H^+ and O^+ beams with decreasing solar illumination is accompanied by a decrease in the outflow rates of conics, i.e., sunlight favors conics while darkness favors beams in the distributions observed at ~8000 km during quiet conditions reported here. The relative variation of beam and conic characteristic energies in these same quadrants is more complex. Finally we note that, in general, the characteristic energies of conic distributions are significantly smaller than those of ion beam distributions.

Table 4 Variations of outflow rates and energies with SZA by quadrant and type

Species	Type	Variation of Outflow Rate				Characteristic Energy (keV)			
		12	18	24	06	12	18	24	06
H^+	All distributions	-	+++	+++	-	*	*	*	*
	Beam	+	+	+++	+++	0.34 +	0.66 -	1.18 +++	0.34 -
	Conic	-	-	+	-	0.06 *	0.20 -	0.18 -	0.16 +
	UFI	-	+	+++	+	0.14 *	0.49 -	0.71 -	0.26 +
O^+	All distributions	-	+	+++	---	0.23 *	0.37 +++	0.43 +++	0.28 -
	Beam	+	+	+++	+	0.23 +	0.56 -	0.88 +	0.48 +
	Conic	-	-	+++	---	0.11 +	0.17 -	0.14 +++	0.13 +
	UFI	-	+	+++	-	0.13 +	0.38 -	0.39 +++	0.22 +
He^+	All distributions	+	+++	+++	+	*	*	*	*
	Beam	+++	+++	+++	+++	0.41 -	0.80 -	0.89 +	0.42 *
	Conic	+	*	+++	*	0.22 *	0.23 *	0.35 *	0.18 -
	UFI	+++	+++	+++	+++	0.32 -	0.67 +++	0.70 *	0.35 -

–: weakly negative dependence; +: weakly positive dependence; ---: strongly negative dependence; +++: strongly positive dependence.
* Noisy and/or ambiguous data

Discussion

The data from the Polar Toroidal Ion Mass-Angle Spectrograph (TIMAS) presented above provide new information on the role that solar illumination plays in energization and transport processes responsible for converting ionospheric thermal plasmas into the cool polar wind and the hotter plasmas in the plasmasphere, plasma sheet, plasma mantle and ring current. In addition, these data provide a comprehensive report on average energies and associated fluxes of escaping ionospheric ions.

The discussion below is organized as follows. After briefly reviewing relevant characteristics of the data presented here, we examine previous work on the influence of solar illumination on ion energization and transport. These include information about seasonal variations in energetic ion outflow (e.g. Yau *et al.,* 1985, 1988), intensification of auroral acceleration processes in darkness (e.g. Newell *et al.,* 1996), and variations in thermal O^+ outflow with solar illumination (e.g. Abe *et al.*, 2004). We then discuss characteristic energies of the outflowing ions and their angular distribution types to explore how they can be used to provide insight into processes responsible for energization and transport.

Summary of observations

We have limited our analysis to solar minimum and geomagnetically quiet intervals characterized by a Dst index greater than –50 nT. The average data presented above do not include observations from magnetic storm intervals during which a significantly larger fraction of the upflowing ionospheric plasma is energized into the TIMAS energy range [e.g. Cladis *et al.*

2000], nor do they reflect significant spatial and temporal variations in the net outflow observed even during relatively geomagnetic quiet times [Peterson *et al.* 2002].

Table 2 and the associated discussion show that the data presented here are consistent with other large-scale estimates of net outflow rates obtained at different altitudes and over different energy ranges from DE-1, Akebono, Polar, and FAST. The consistency of the total O^+ outflow rates with those derived from Akebono is significant because it shows that the net outflow rates derived from TIMAS perigee data presented here are reliable lower limits to the average net outflow rates, including the polar wind component, which is prevalent during solar and geomagnetic quiet intervals. Because fluxes observed below 15 eV are not included in calculating average energy, the average energies reported in Tables 3 and 4 are upper limits. Table 2 shows that, at 8,000 km, a larger fraction of the outflowing O^+ than H^+ ions observed from Akebono ions has been energized into the TIMAS energy range of 15 eV to 33 keV. Two conclusions can be drawn from Table 2. Energization of thermal plasmas occurs at all altitudes, including those above the ~8,000 km surveyed here; and the energization rates for O^+ and H^+ as a function of altitude are significantly different.

The data in Tables 2 and 3 show that the cusp is quantitatively an important but not dominant source of ionospheric O^+ plasma for the magnetosphere. The global average outflow rates derived from Akebono reported by Cully et al. [2003a] have been corrected for variations in the spacecraft potential; they include average thermal O^+ plasmas observed at similar altitudes to those reported here. The differences between the Akebono and Polar/TIMAS derived global outflows reported in Table 2 are small and consistent with the Akebono upper energy limit of ~70 eV missing a fraction of the upflowing O^+ flux. The high values of global O+ outflow reported at Polar apogee by Lennartsson et al. [2004] imply a continued acceleration of O^+ ions with energies below the TIMAS cutoff energy of 15 eV at altitudes above 8,000 km. Because of the relatively high lower energy cut off of the TIMAS instrument we can not use the data in Table 3 to quantitatively estimate the total percentage O^+ outflow from the cusp, or the data in Table 2 to estimate global H^+ outflow rate. We note also that the observations reported here are from intervals where the Dst index is below 50 nT. During storm times significantly higher fluxes of O^+ are observed in the cusp region [e.g. Moore et al. 1999b].. There are insufficient data available to asses the local time distribution of O^+ during storm times

Influence of solar illumination on energization and transport

To address the effects of variations of solar illumination on energization and transport processes, average net outflows and energies were calculated as a function of solar zenith angle (SZA) and magnetic local time quadrant for all of the data and for three angular distribution types (i.e. beam, conic, and upflowing ion (UFI) distribution). Sorting by solar zenith angle allows us to examine the influence of solar variability on a finer time scale than previous seasonal studies. Sorting by magnetic local time sector, solar zenith angle, and angular distribution type, as discussed below, allows us to examine the differences in the influence of solar variability on energization processes acting on the dayside and night side of the auroral oval.

Seasonal variations in the occurrence of upflowing O^+, but not H^+, UFI events were reported by Yau et al. [1985]. Variations in O^+, but not H^+ upflowing fluxes as a function of solar activity were reported by Yau et al. [1988]. The strong variations in He^+ outflows as a function of solar illumination reported above are easily explained by the well-known seasonal variation in He^+ ionospheric densities [e.g., Peterson *et al.*, 2001]. Figure 5a shows that the global average outflow rates of both H^+ and O^+ at Polar perigee do not depend strongly on solar illumination during the solar and geomagnetically quiet conditions considered here. Table 4 shows variations in H^+ and O^+ outflows in various MLT quadrants as a function of solar illumination. In the midnight quadrant, the net outflow rates of all ions increase with decreasing solar illumination. In some other MLT quadrants the H^+ and/or O^+ rates decrease with decreasing solar illumination. Significant increases of polar wind outflows with increasing solar illumination have been reported by Horita et al. [1993], Su et al. [1998], Abe et al. [2004] and others. The relatively weak increases in H^+ and O^+ outflowing fluxes on the dayside shown in Table 4 are a result of the 15 eV TIMAS energy threshold. Table 3 shows that the distribution of net outflows in the various MLT quadrants is different for H^+ and O^+, with more O^+ outflow in the noon quadrant and more H^+ outflow in the midnight quadrant. Locally, especially in the midnight sector, variations in solar illumination have dramatic effects on ion outflow fluxes and energies. The conclusion we draw from these observations is that variations in the solar EUV and geomagnetic energy inputs into the ionosphere, rather than heating and cooling of the ionosphere on a seasonal time scale, primarily determine the global rates of H^+ and O^+ outflow.

Newell *et al.* [1996] established that the intensity of the auroral acceleration process occurring in the evening MLT sector was significantly modulated by solar illumination. Collin *et al.* [1998] examined the occurrence frequency of ion beams in the 18-24 MLT sector from 18 months of TIMAS perigee data sorted into summer and winter seasons. They reported a significant increase in the frequency of ion beams (but not conics) in data acquired during the winter (dark) season. Collin *et al.* reviewed related observations of electron precipitation [Newell *et al.*, 1996], UV aurora [Liou *et al.* 1997], AKR [Kumamoto and Oya 1998], and EMIC radiation [Erlandson and Zanetti 1998] that all show the same seasonal dependence. Collin *et al.* [1998] concluded that solar EUV and, by implication, ionospheric conductivity modulate the auroral acceleration process responsible for creating ion beams. Figure 5b shows that, on average, H^+ and O^+ characteristic energies increase with decreasing solar illumination. The observations reported in Table 4 extend this conclusion to all other local times.

The primary auroral acceleration process is characterized by the upflowing ion beams seen above ~ 6,000 km [e.g. Shelley and Collin, 1991]. Figure 4 illustrates the increases in intensity and extent of nightside beam distributions with decreasing solar illumination. Table 4 demonstrates that the outflow rates of ion beams and conics for all species increase with decreasing solar illumination in the midnight quadrant. A different relationship between beams and conics as a function of solar illumination is shown for the noon, dawn, and dusk MLT quadrants. In these quadrants the outflow rate of H^+ and O^+ beams (conics) increases (decreases) with decreasing solar illumination. Since ion conics produced at low altitudes cannot be distinguished from beams at high altitude, we suggest that the anti-correlation of solar illumination dependence of beam and conic outflow rates is yet another indication of variations in the altitude at which auroral acceleration processes occur. See, for example, Yau *et al.* [1985], Collin *et al.* [1998], and Newell *et al.* [1996]. We can only speculate why this beam/conic

relationship with solar illumination does not extend to the midnight quadrant. Perhaps it is related to the extra energy input to the ionosphere associated with substorms.

Solar illumination is especially important in the energization and transport of thermal ionospheric O^+. Thermal O^+ is created on the dayside and transported into the nightside ionosphere by large-scale ionospheric convection. Thermal O^+ in the F-region ionosphere has to acquire at least a velocity of 11 km/s, or 10 eV energy, in order to overcome the Earth's gravitational potential and reach the plasma sheet and outer magnetosphere (See, for example, Seki *et al.* 2000). In principle thermal O^+ energization could occur uniformly in local time. However, Horita *et al.* [1993] reported, and Zeng *et al.* [2004] confirmed, the existence of a day/night asymmetry in upflowing thermal plasmas observed by Akebono and Polar. Subsequent analysis of Akebono thermal plasma ($0 < E/q < 70$ eV) data by Abe and his co-workers have confirmed the preference for dayside energization of O^+ and suggested that intensifications of the ambi-polar electric field generated by escaping photoelectrons provides the energy primarily responsible for preferential day side energization of O^+. See Abe *et al.* [2004] and references therein.

The energetic O^+ data presented above and discussed below are consistent with the conclusion that the dayside (sunlit) hemisphere is the origin of most escaping O^+. Table 2 summarizes previous reports of average global ion outflow obtained from DE-1, Polar, FAST, and Akebono at various altitudes and over various energy ranges. It shows that globally at least half of the O^+ flux reaching higher altitudes is below the TIMAS energy-per-charge threshold of 15 V plus the spacecraft potential. It can be readily inferred from Table 3 that the largest fraction of energetic O^+ that is not identified as UFI, and therefore with intensity less than 10^{10} ions/m^2-s-sr, appears in the noon quadrant. Together with the Horita *et al.* [1993] and Zeng *et al.* [2004] results, these observations suggest that the bulk of the escaping O^+ that is not detected by TIMAS is coming primarily from the noon MLT quadrant. We note that Moore *et al.* [1999b], Strangeway *et al.* [2000], and Cladis *et al.* [1999] and others have demonstrated that during large geomagnetic storms, which are not included in the data summarized in this paper, significantly more energetic O^+ originates in the noon quadrant than is reported here.

Before we begin a discussion of the characteristic energies of outflowing ions reported above, we note that the net outflow rate of He^+ reported in Table 1 is significantly lower than that derived from the same data set and reported by Peterson *et al.* [2001]. As discussed above, we believe the analysis of Peterson *et al.* [2001] did not sufficiently take into account the effects of the reduced energy and angular resolution of the He^+ data (due to telemetry rate restrictions) on the magnitude of the required correction for downflowing plasma-sheet energetic He^+ ion fluxes. We also pointed out in the discussion of Figure 3 large regions of downflowing ions that were observed on the dusk side of the magnetosphere under sunlit conditions, and on the dawn side under darkness. There have been previous reports of downflowing thermal ions associated with the "auroral ion fountain" [see, for example, Horwitz and Lockwood, 1985 or Loranc et al., 1990.] These papers are discussing downflowing thermal ions inside the polar cap. The downflowing ions apparent in Figure 3 are non-thermal and occur equatorward of the auroral oval and are thus not related to the "auroral ion fountain." We have no explanation for this interesting variation.

Characteristic energies of outflowing ions

Few large-scale surveys of the characteristic energy of outflowing ions have been published. Ghielmetti et al. [1987] examined the characteristic energies and fluxes of H^+ and O^+ ion beams above 500 eV. Most other previous reports on energy have been qualitative assessments of specific regions. For example the Moore *et al.* [1986] report of a characteristic energy (10 eV) and temperature (100,000^o K) for O^+ in the cusp have been generally accepted and used for large scale modeling purposes. Characteristic energies of upflowing auroral ion beam distributions derived from specific event studies have been reported from several missions by the Lockheed and Kiruna groups. These works have been reviewed and summarized by Shelley and Collin [1991], Yau and André [1997] and Moore *et al.* [1999a]. Abe *et al.* [2004] have reported the solar activity dependence and seasonal variation of H^+ and O^+ polar wind velocity profiles observed by the suprathermal ion mass spectrometer (SMS) on Akebono. These observations spanned a solar cycle and covered a wide range of altitudes and invariant latitudes (ILAT) in the polar ionosphere as well as a variety of geomagnetic activity conditions in the altitude range from 1,500 to 8,500 km.

Recently Lennartsson *et al.* [2004] and Andersson *et al.* [2005] have reported characteristic energies observed from energetic ion mass spectrometers on the Polar and FAST satellites respectively. Lennartsson *et al.* reported characteristic energies for H^+ and O^+ during intervals of strong northward or southward interplanetary magnetic field (IMF). Significantly higher H^+ energies were observed during intervals of strong IMF northward at Polar perigee. The mean energies reported were ~1.5 keV and ~0.3 keV at ~8,600 km (Polar perigee) and ~2.0 keV and ~1.5 keV at ~50,000 km (Polar apogee) for H^+ and for O^+, respectively. As noted above, the average energy estimates for H^+ at perigee reported by Lennartsson *et al.* [2004] are subject to significant errors because of the required correction for precipitating energetic particle fluxes (the so-called loss cone correction). Andersson *et al.* calculated characteristic energy for O^+ in three altitude ranges between 1,500 and 4,200 km from FAST. They avoided the problem of the loss cone correction by considering only O^+ and limiting the energy range over which the O^+ energy was calculated. Anderson *et al.* noted increasing values of global upflowing fluxes in the three altitude ranges considered, indicating energization of a thermal, polar wind, O^+ component into the FAST energy range (3 eV – 12 keV). They demonstrated that the altitude dependence of the characteristic O^+ energy is distinctly different in the noon, midnight, and dusk and dawn MLT quadrants. They noted that this implies that either different physical processes are dominant, or the altitude dependences of these processes and the transport of ions are different in these MLT quadrants. In the highest altitude range the characteristic O^+ energies in the noon, dusk, midnight, and dawn MLT quadrants were ~30 eV, 10 eV, 70 eV and 30 eV, respectively. We conclude that it is not physically justified to characterize ion outflow at Polar perigee altitude by a single characteristic energy.

In Table 3 we have reported characteristic energies as a function of local time and ion angular distribution type. We defined three angular distribution types: beams, conics, and UFI, which we define here as the combination of beams and conics. Note that our definition of conics does not include distributions with angular peaks at 90^o because they are easily confused with trapped distributions. Peterson *et al.* [1992] have established that most conics at ~8,000 km have pitch angles well away from 90^o, so only a small fraction of upflowing conics are not included

here. Table 3 increases what is known about characteristic energies of outflowing ions as a function of mass and angular distribution type. In specific cases noted below these data contradict previous results.

The characteristic energies reported for H^+ in Table 3, except for the beam energy in the midnight MLT quadrant, are significantly lower than those reported by Lennartsson *et al.* [2004]. However, the energy values given in Table 1 are consistent with those reported by Lennartsson *et al.* As noted in the discussion of Table 1, the variation of He^+ characteristic energy with the cutoff invariant latitude in the analysis indicates that errors associated with the loss cone correction significantly biased the calculated energy for cut off latitudes of 55^o and 60^o. Investigation of the calculated average H^+ energy as a function of cut off latitude and MLT sector, not presented here, leads us to conclude that the calculated H^+ energy flux (and therefore the characteristic energy) may be significantly biased upward also because of intense fluxes of precipitating and trapped energetic H^+. The H^+ and He^+ characteristic energies for the full data set (i.e. all distributions) are therefore not reported in Figure 4 and Tables 3 and 4. However, note that UFIs only constitute 67% of the H^+ net outflow (and 55% for He^+) in Table 3. The flux of precipitating and trapped energetic O^+ ions is significantly less than that of H^+ and the error introduced by the loss cone correction is also significantly less. We note that the O^+ characteristic energies from the different angular distributions types in Table 3 are all less than 1 keV.

The characteristic O^+ energies in Table 3 are higher than those reported from FAST at lower altitudes (~3,000 km) by Andersson *et al.* [2005]. For O^+, the latter are a factor of ~10, ~40, ~5, and ~10, larger in the noon, dusk, midnight, and dawn quadrants, respectively. In the dusk quadrant, the characteristic energy increased from 10 eV at the FAST altitude (3,000-4,200 km) to about 400 eV at the Polar altitude (8,600 km). We note that these energies include a significant contribution from O^+ ion beams, indicating relatively more beam producing processes acting in the dusk MLT quadrant between the altitudes sampled by FAST and Polar.

Contrary to the results of Collin *et al.* [1987] and others reviewed by Shelley and Collin [1991], the characteristic O^+ beam energy in Table 3 is lower than that of H^+ except in the dawn (06) MLT quadrant. The investigations reviewed by Shelley and Collin [1991] were based on ion beam events that were carefully selected by visual means. We believe the reason for our contradictory results on relative O^+ and H^+ beam energies is due to both the less precise method used to identify ion beams in this study and to differences between the event based studies and the long-term averages presented here.

Further information about ionospheric energization processes can be obtained by examining relative fluxes and energies of beam and conic distributions. As noted above identification of beam and conic distributions is instrument specific. Here, identification of beam, conic and UFI distributions requires the existence of a statistically meaningful peak in an ion distribution. Detecting such peaks requires setting a relatively high threshold (10^{10} ions/m^2-s-sr) below which distributions are not considered. Distributions below this TIMAS instrument specific threshold could have undetectable beam, conic or UFI characteristics, or they could be the high energy "tails" of thermal distributions extending into the TIMAS energy range.

Ion beams are generally associated with acceleration regions of intense and primarily upward currents, and ion conics are often associated with downward currents, but the differences are not that clearly defined, as discussed in Moore *et al.* [1999a]. Yau *et al.* [1985] concluded from a study of data from DE-1 that O^+ UFI events were more common in summer than in winter. They also noted that the proportion of O^+ conics increased in summer. Yau *et al.* did not find significant variations of upflowing H^+ UFI events in the DE-1 data set. Øieroset *et al.* [1999] investigated low energy (40 eV – 1.2 keV) upflowing ions from 70 dayside passes of the Viking satellite in the altitude range 6,000 – 13,500 km. They found conics dominating the upflowing flux in the cusp region and beam fluxes dominating the pre and post noon sectors.

Conic distributions are created by processes that transfer energy to the ions in a direction perpendicular to the local magnetic field. Beam distributions may be created either by the same processes at much lower altitude or by processes that act primarily in the magnetic field direction. Figure 3 and Table 3 show that the characteristic energy of beam distributions is greater than that of conic distributions, consistent with earlier episodic reports. Table 3 shows that upflowing fluxes associated with conic distributions are enhanced in the cusp region, especially for O^+, while fluxes associated with ion beams are enhanced in the midnight sector, especially for H^+. Characteristic energies are lowest in the cusp and highest in the midnight sector. We conclude that the dominant ion energization and/or transport processes are significantly different in the cusp and midnight regions.

In this paper we have concentrated on characterizing the flux, energy, and angular distributions of escaping ionospheric ions at ~ 8,000 km observed by the Polar TIMAS instrument. We have not focused on the diverse and complex processes responsible for the energization and transport of thermal ionospheric plasmas to 8,000 km. As noted in the introduction, progress in understanding these processes has been slow because of the complexity of the problem. Progress can be made perhaps by incorporating the results presented here with large-scale modeling that includes parameterizations of the basic plasma physical processes in a manner similar to that introduced by Strangeway et al. [2005] and Zeng et al. [2005] but focusing on non-storm time intervals and including observations from all local time sectors.

Conclusions

We have examined as a function of solar illumination characteristic energies and upflowing fluxes of energetic (15 eV < E/q < 33 keV) ionospheric ions entering the Earth's magnetosphere during non-storm times (Dst greater than -50 nT). The data were obtained from the Polar TIMAS instrument during 1996-1998 (solar minimum) at an altitude of ~8000 km. The major findings are:

- The effects of solar illumination on ion energization and transport are more rapid than the seasonal time scales previously suggested.
- Solar illumination modulates auroral acceleration processes in all magnetic local time sectors, not just the evening sector as previously established.
- Different ionospheric plasma energization and/or transport mechanisms are dominant in the cusp and midnight sectors.

- The cusp is quantitatively an important but not dominant source of ionospheric O^+ plasma for the magnetosphere during non-storm times.
- We have reported realistic upper limits of characteristic energies of upflowing H^+, O^+ and He^+ that vary as a function of magnetic local time (MLT) and angular distribution type.
- The energization of thermal plasmas occurs at all altitudes and, in the region between the ionosphere and 8,000 km, O^+ is energized faster than H^+.
- Large regions of downflowing ions on the dusk (dawn) side of the magnetosphere equatorward of the auroral oval under sunlit (dark) conditions are found. These features are distinctly different from downward flowing thermal ions observed in the polar cap and associated with the auroral ion fountain. We have no explanation for these unexpected features.

Understanding the role ionospheric plasmas play in magnetospheric processes such as the dayside reconnection rate, ULF pulsations and ring current energization processes and the onset and frequency of substorms is a major long term goal of magnetospheric research. Magnetospheric processes are so complex, and the magnetospheric volume so large, that observations such as those reported here cannot directly address them. These observations must be supplemented by comprehensive and large-scale magnetospheric models that include the effects of ionospheric plasma energization and transport. Perhaps the most important results from this analysis are the data on characteristic energies and upflowing fluxes reported in Tables 3 and 4. These data are necessary to validate large-scale magnetospheric models that include ionospheric plasma energization and transport.

Acknowledgements: We recognize Ed Shelley who conceived and implemented the TIMAS instrument. WKP thanks Chris Cully and Laila Andersson for helpful comments. This research was sponsored by NASA Grant NNG05GE64G at the University of Colorado, and NASA Contract NAS5-30302 at Lockheed Martin, and supported by the Canadian Space Agency (CSA) and the Natural Science and Engineering Research Canada (NSERC) at the University of Calgary. The authors thank the referees for constructive comments.

References:

Abe, T., A.W. Yau, S. Watanabe, M.Yamada, and E. Sagawa (2004), Long-term variation of the polar wind velocity and its implication for the ion acceleration process: Akebono/suprathermal ion mass spectrometer observations*, J. Geophys. Res., 109*, A09305, doi:10.1029/2003JA010223.

Andersson, L., W.K. Peterson, and K.M. McBryde (2005), Estimates of the suprathermal O+ outflow characteristic energy and relative location in the auroral oval, *Geophys. Res. Lett., 32*, L09104, doi:10.1029/2004GL021434.

André, M. and A.W. Yau (1997), Theories and Observations of Ion Energization and Outflow in the High Latitude Magnetosphere, *Space Science Reviews, 80*, 27.

Ashour-Abdalla, M., M. El-Aloui, V. Peroomian, R.J. Walker, J. Raeder, L.A. Frank, and W.R. Paterson (2000), The origin of the near-Earth plasma population during a substorm on November 24, 1996, *J Geophys. Res., 105*, 2589.

Chappell, C.R., T.E. Moore, and J.H. Waite, Jr. (1987), The ionosphere as a fully adequate source of plasma for the Earth's magnetosphere, *J. Geophys. Res., 92*, 5896.

Chen, S.-H., and T. E. Moore (2004), Dayside flow bursts in the Earth's outer magnetosphere, *J. Geophys. Res.*, *109*, A03215, doi:10.1029/2003JA010007.

Cladis, J.B., H.L. Collin, O.W. Lennartsson, T.E. Moore, and C.T. Russell (2000), Observations of Centrifugal Acceleration of Ions during Compression of the Magnetosphere, *Geophysical Research Letters, 27*, 7915.

Collin, H.L., W.K. Peterson, and E.G. Shelley (1987), Solar cycle variations of some mass dependent characteristics of upflowing beams of terrestrial ions, *J. Geophys. Res., 92*, 4757.

Collin, H.L., W.K. Peterson, J.F. Drake, and A.W. Yau (1988), The Helium Components of Energetic Terrestrial Ion Upflows: Their Occurrence, Morphology, and Intensity, *J. Geophys. Res., 93*, 7558.

Collin, H.L., W.K. Peterson, O.W. Lennartsson, and J.F. Drake (1998), The seasonal variation of auroral ion beams, *Geophys. Res. Lett., 25*, 4071.

Cully, C.M., E. F. Donovan, A. W. Yau, and G. G. Arkos (2003a), Akebono/Suprathermal Mass Spectrometer observations of low energy ion outflow: Dependence on magnetic activity and solar wind conditions, *J. Geophys. Res., 108*(A2), 1093, doi: 10.1029/2001JA009200.

Cully, C.M., E. F. Donovan, A. W. Yau, and H. J. Opgenoorth (2003b), Supply of thermal ionospheric ions to the central plasma sheet, *J. Geophys. Res.*, *108*(A2), 1092, doi:10.1029/2002JA009457.

Elkington, S. R., M. K. Hudson, and A. A. Chan (2003), Resonant acceleration and diffusion of outer zone electrons in an asymmetric geomagnetic field, *J. Geophys. Res.*, *108*(A3), 1116, doi:10.1029/2001JA009202.

Erlandson, R.E., and L. J. Zanetti (1998), A statistical study of auroral electromagnetic ion cyclotron waves, *J. Geophys. Res., 103*, 4627.

Fraser, B. J., J. L. Horwitz, J. A. Slavin, Z. C. Dent, and I. R. Mann (2005), Heavy ion mass loading of the geomagnetic field near the plasmapause and ULF wave implications, *Geophys. Res. Lett.*, *32*, L04102, doi:10.1029/2004GL021315.

Ghielmetti, A.G., E.G. Shelley, and D.M. Klumpar (1987), Correlation between number flux and energy of upward flowing ion beams. *Physica Scripta*, 36, 362.

Horita, R.E., A.W. Yau, B.A. Whalen, A. Abe, and S. Watanabe (1993), Ion depletion zones in the polar wind: EXOS D Suprathermal Ion Mass Spectrometer observations in the polar cap, *J. Geophys. Res. 98*, 11439.

Horwitz, J.L., and M. Lockwood (1985), The cleft ion fountain: A two dimensional kinetic model, *J. Geophys. Res.*, 90, 9749.

Hultqvist, B., M. Øieroset, G. Paschmann, and R. Treumann (Eds.) (1999), *Magnetospheric plasma sources and losses*, Kluwer Academic Publishers, Dordrecht, Boston, London.

Huddleston, M. M., C.R. Chappell, D.C. Delcourt, T.E. Moore, B.L. Giles, and M.O. Chandler (2005), An examination of the process and magnitude of ionospheric plasma supply to the magnetosphere, *J. Geophys. Res*., doi:1029/2004JA010401, in print

Johnson, R.G. (1983), *Energetic ion composition in the Earth's magnetosphere*, Terra Scientific Publishing, Tokyo and Reidel Publishing, Dordrrecht, Boston, and London.

Kistler, L. M., *et al.* (2005), Contribution of nonadiabatic ions to the cross-tail current in an O^+ dominated thin current sheet, *J. Geophys. Res.*, *110*, A06213, doi:10.1029/2004JA010653.

Kumamoto, A., and H. Oya (1998), Asymmetry of occurrence-frequency and intensity of AKR between summer polar region and winter polar region sources, *Geophys. Res. Lett., 25*, 2369.

Lennartsson, O.W., H. L. Collin, and W. K. Peterson (2004), Solar wind control of Earth's H^+ and O+ outflow rates in the 15-eV to 33-keV energy range, *J. Geophys. Res., 109*, A12212, doi:10.1029/2004JA010690.

Liou, K., P.T. Newell, C-I. Meng, M. Brittnacher, and G. Parks (1997), Synoptic auroral distribution: a survey using POLAR ultraviolet imagery, *J. Geophys. Res., 102*, 27197.

Loranc, M., R.A. Heelis, W.B. Hanson, and J.-P. St.-Maurice (1990), A morphological study of vertical ionospheric flows in the high-latitude F Region, *J. Geophys. Res*., 96, 3627.

Moore, T.E., M. Chandler, J.H. Waite Jr., C.R. Chappell, A. Persoon, and M. Sugiura (1986), Upwelling O^+ ion source characteristics, *J. Geophys. Res., 91*, 7019.

Moore, T.E., R. Lundin, D. Alcayde, M. André, S.B. Ganguli, M. Temerin, and A. Yau (1999a), Source Processes in the High-Latitude Ionosphere, *Space. Sci. Rev., 88*, 7.

Moore, T.E., W.K. Peterson, C.T. Russell, M.O. Chandler, M.R. Collier, H.L. Collin, R. Fitzenreiter, B.L. Giles, and C.J. Pollock (1999b), Ionospheric Mass Ejection in Response to a Coronal Mass Ejection, *Geophysical Research Letters, 26*, 2339.

Newell, P.T., C-I. Meng, and K.M. Lyons (1996), Suppression of discrete aurora by sunlight, *Nature, 381*, 766.

Øieroset, M., M. Yamauchi, L. Liszka, and B. Hultqvist (1999), Energetic ion outflow from the dayside ionosphere: Categorization, classification, and statistical study, *J. Geophys. Res., 104*(A11), 24,915–24,928.

Peterson, W.K., H.L. Collin, M.F. Doherty, and C.M. Bjorklund (1992), O^+ and He^+ restricted and extended (bi-modal) ion conic distributions*, Geophys. Res. Lett., 19*, 1439.

Peterson, W.K, H.L. Collin, A.W. Yau, and O.W. Lennartsson (2001), Polar/TIMAS Observations of Suprathermal Ion Outflow During Solar Minimum Conditions. *J. Geophys. Res., 106*, 6059.

Peterson, W.K., H.L. Collin, M. Boehm, A.W. Yau, C. Cully, and G. Lu (2002), Investigation into the Spatial and Temporal Coherence of Ionospheric Outflow on January 9-12, 1997*, J. Atmos. and Solar Terr. Phys., 64*, 1659.

Shelley, E.G., and H.L. Collin (1991), Auroral ion acceleration and its relationship to ion composition, in *Auroral Physics*, C.-I. Meng, M.J. Rycroft, and L.J. Frank Eds., pg129, Cambridge University Press, New York.

Seki, K., R.C. Elphic, M.F. Thomsen, J. Bonnell, E.J. Lund, M. Hirahara, T. Terasawa, and T. Mukai (2000), Cold flowing O^+ beams in the lobe/ mantle at Geotail: Does FAST observe the source?, *J. Geophys. Res., 105*, 15,931.

Seki, K., *et al.* (2003), Cold ions in the hot plasma sheet of Earth's magnetotail, *Nature, 422*, 589.

Su, Y., J. L. Horwitz, T. E. Moore, B. L. Giles, M. O. Chandler, P. D. Craven, M. Hirahara, and C. J. Pollock (1998), Polar wind survey with the Thermal Ion Dynamics Experiment/Plasma Source Instrument suite aboard POLAR, *J. Geophys. Res.*, *103*(A12), 29,305.

Strangeway, R.J., C.T. Russell, C.W. Carlson, J.P. McFadden, R.E. Ergun, M. Temerin, D. M. Klumpar, W.K. Peterson, and T.E. Moore (2000), Cusp field-aligned currents and ion outflows, *J. Geophys. Res.*, *105*(A9), 21,129–21,142.

Strangeway, R.J., R.E. Ergun, Y.-J. Su, C.W. Carlson, and R.C. Elphic (2005), Factors controlling ionospheric outflows as observed at intermediate altitudes, *J. Geophys. Res., 110*, A03221, doi:10.1029/2004JA010829.

Winglee, R.M. (2003), Circulation of ionospheric and solar wind particle populations during extended southward interplanetary magnetic field, *J. Geophys. Res.*, *108*(A10), 1385, doi:10.1029/2002JA009819.

Yau, A.W., B.A. Whalen, W.K. Peterson, and E.G. Shelley (1984), Distribution of Upflowing Ionospheric Ions in the High-Altitude Polar Cap and Auroral Ionosphere, *J. Geophys. Res., 89*, 5507.

Yau, A.W., P.H. Beckwith, W.K. Peterson, and E.G. Shelley (1985), Long-term (solar cycle) and seasonal variations of upflowing ionospheric ion events at DE 1 altitudes, *J Geophys. Res., 90*, 6395.

Yau, A.W., W.K. Peterson, and E.G. Shelley (1988), Quantitative Parameterization of Energetic Ionospheric Ion Outflow, in *Modeling Magnetospheric Plasma*, *Geophysical Monograph 44*, American Geophysical Union, Washington, D. C.

Yau, A.W., and M. André (1997), Sources of ion outflow in the high latitude ionosphere, *Space Sci. Rev., 80*, 1.

Zeng, W., J. L. Horwitz, P. D. Craven, F. J. Rich, and T. E. Moore (2004), The O^+ density trough at 5000 km altitude in the polar cap, *J. Geophys. Res.*, *109*, A03220, doi:10.1029/2003JA010210.

Zeng, Y., T. E. Moore, F. S. Mozer, C. T. Russell, and R. J. Strangeway (2004), Polar study of ionospheric ion outflow versus energy input, *J. Geophys. Res.*, *110*, A07210, doi:10.1029/2004JA010995.

Figure 1

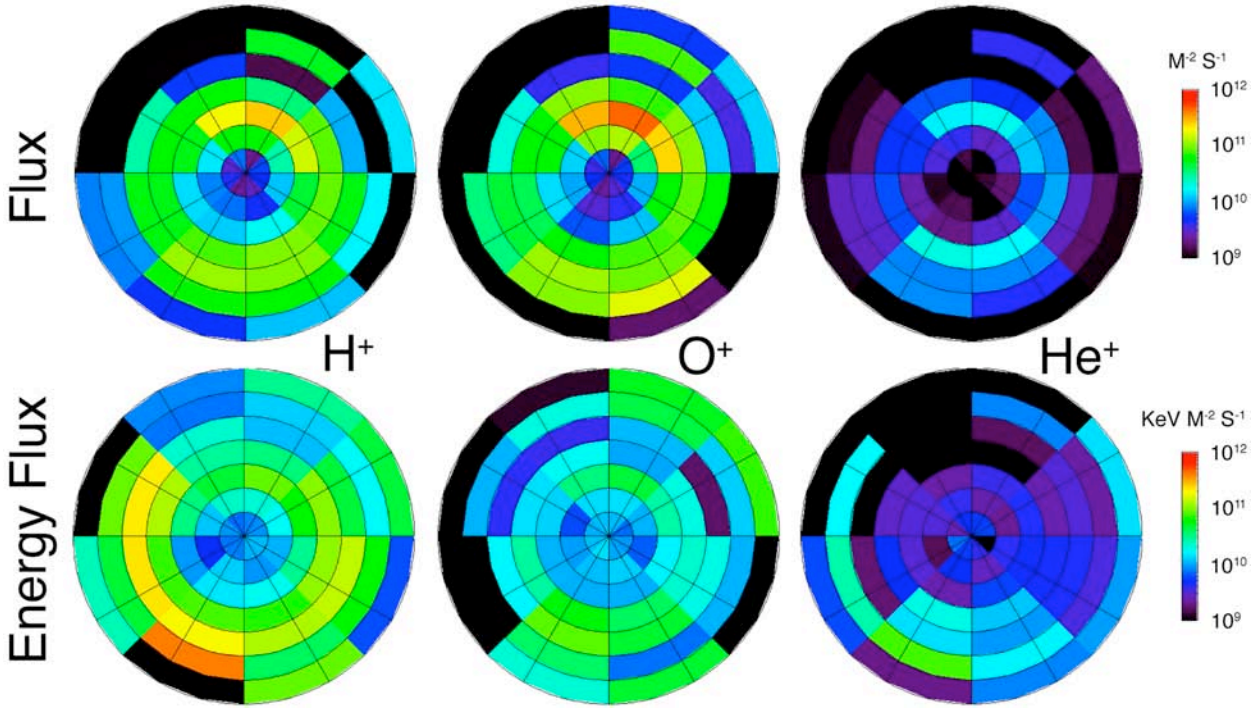

Figure 1. Averaged distributions of H^+ (left), O^+ (middle), and He^+ (right) number (top) and energy flux (bottom panel) observed by TIMAS during Polar perigee passes below 9000 km altitude from March 1996 to December 1998, and normalized to an altitude of 300 km. Data are presented as a function of magnetic local time and invariant latitude, which ranges from 55^o to 90^o in 5^o bins; noon is at the top of each dial and dusk is on the left. The color bars on the right indicate the number flux in units of m^{-2} s^{-1} and energy flux in keV m^{-2} s^{-1}.

Figure 2

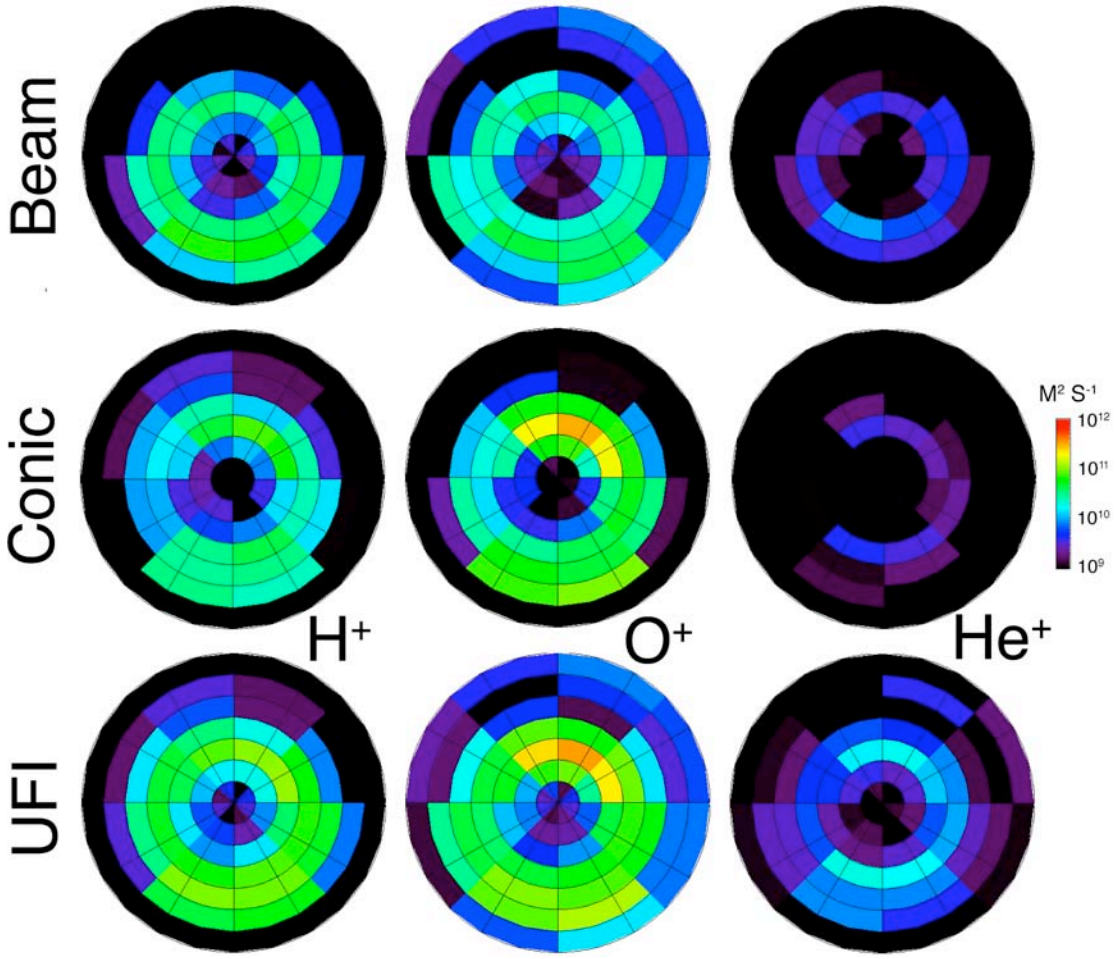

Figure 2: Magnetic local time (MLT) vs. invariant latitude displays of upflowing fluxes of H^+, O^+ and He^+ for the beam, conic and UFI angular distribution types described in the text. The format of the displays is identical to that of Figure 1.

Figure 3

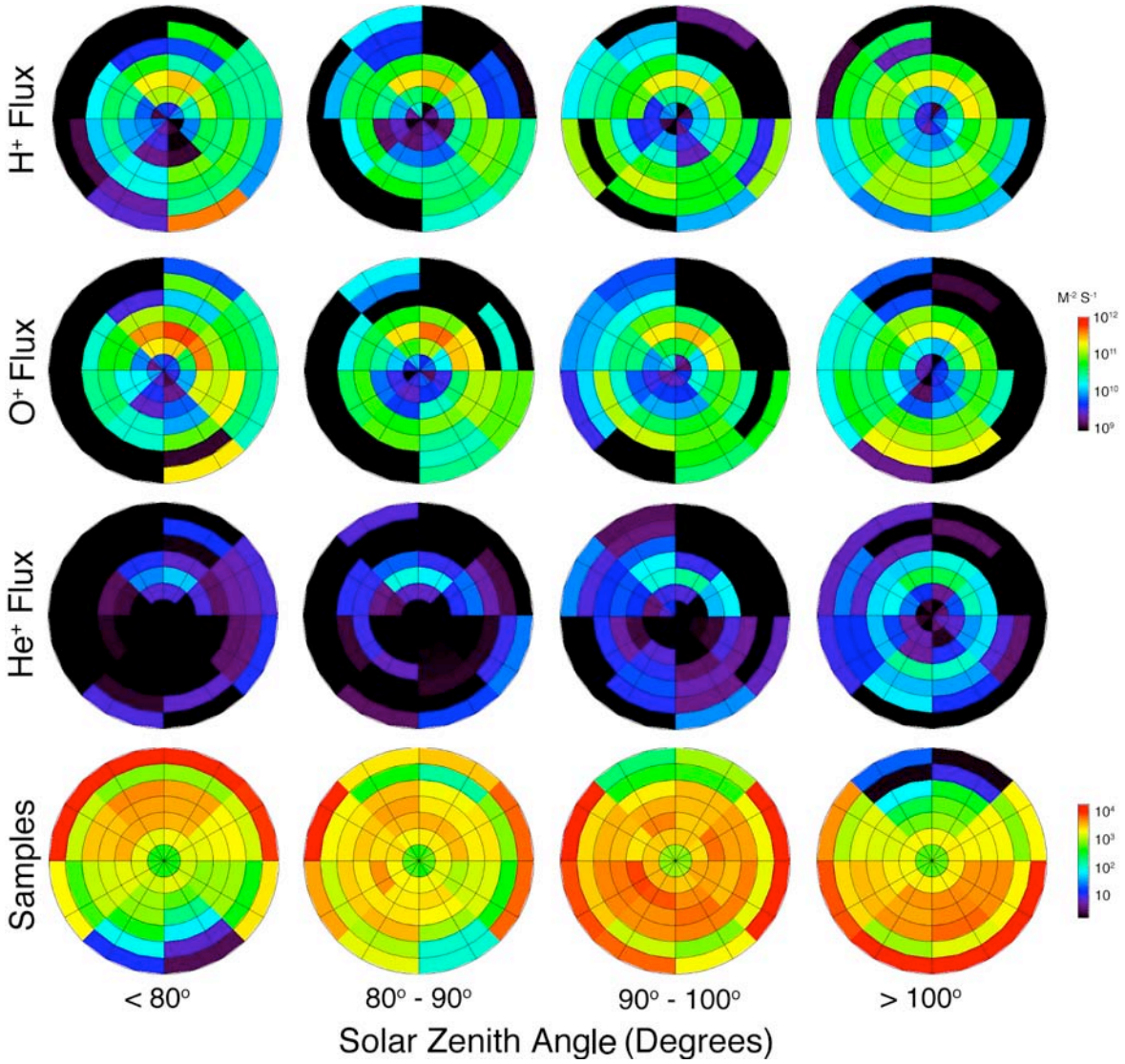

Figure 3: Averaged upward flux of H^+, O^+, He^+ (top 3 panels) and number of data samples (bottom panel) observed by TIMAS on Polar in different ranges of solar zenith angle (SZA) at the magnetic footprint of Polar, as a function of invariant latitude and MLT. From left to right: $0 < SZA < 80$, $80 < SZA < 90$, $90 < SZA < 100$ and $100 < SZA < 180$. Invariant latitude and magnetic local time displays are the same as in Figure 1. Flux units are m^{-2} s^{-1}.

Figure 4.

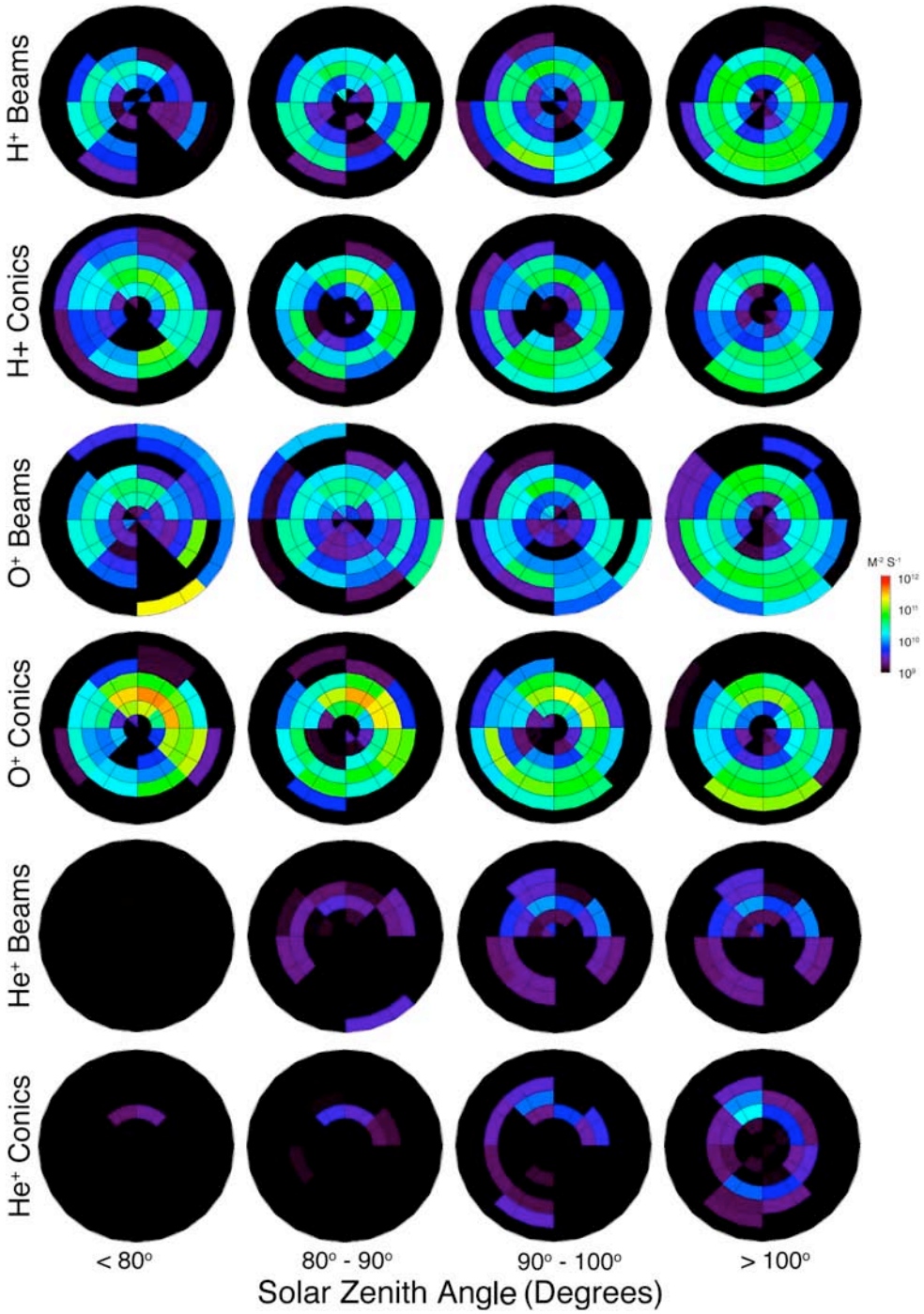

Figure 4 Average number flux distributions of $H^{+,}$ O^{+} and He^{+} beams and conics observed by TIMAS during Polar perigee passes for different ranges of SZA at the magnetic footprint of Polar. Data display format in each panel and SZA range in each column are the same as in Figure 3.

Figure 5a

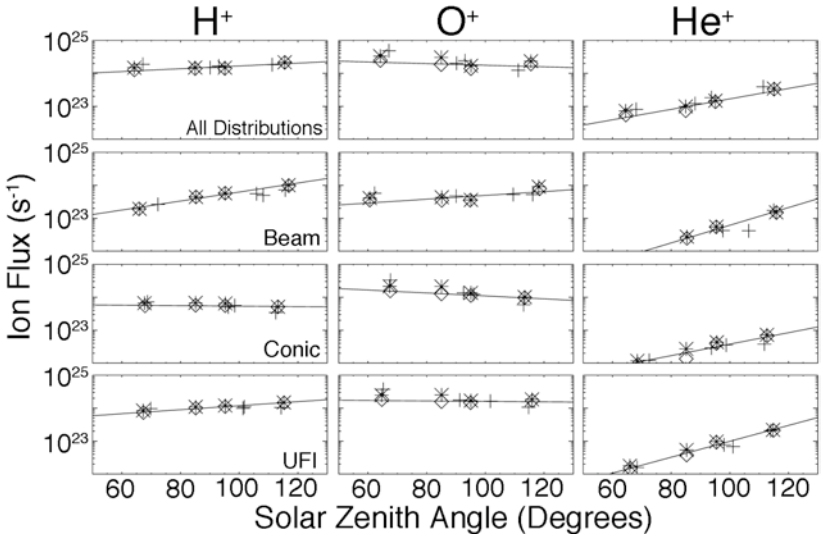

Figure 5a. Average net hemispheric ion outflow rate of H^+, O^+, He^+ (from left to right) observed by TIMAS on Polar, including all data samples (irrespective of their angular distributions) and only beam, conic, and UFI distributions, respectively (from top to bottom), as a function of averaged SZA at the magnetic footprint of the Polar satellite. Diamond: quiet-time (Dst > -50 nT) data; asterisk (*): full data set; plus (+): seasonal data within ±30 days of solstice or equinox; straight line: fits to quiet-time data; see text.

Figure 5b

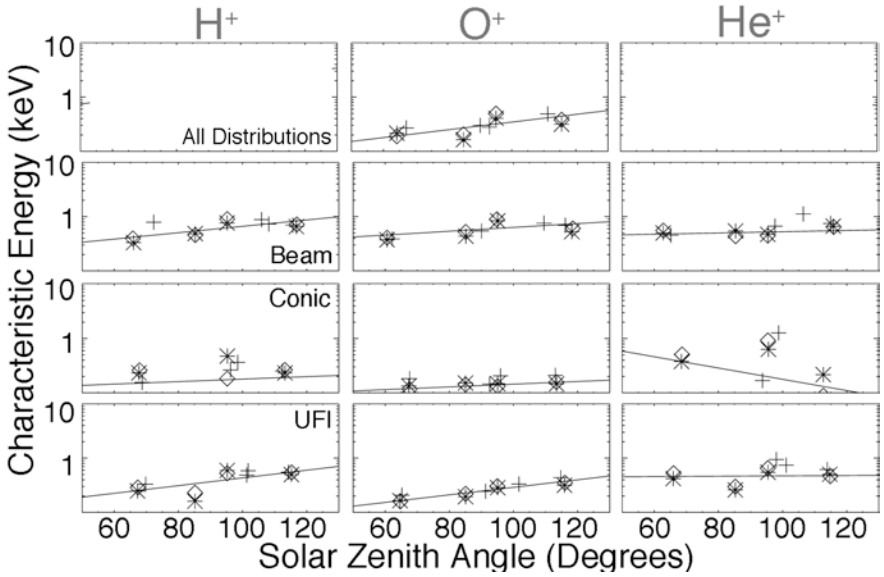

Figure 5b. Average characteristic energy of H^+, O^+, He^+ (from left to right) observed by TIMAS on Polar, including all data samples (irrespective of their angular distributions), beam, conic, and UFI distributions, respectively (from top to bottom), as a function of averaged SZA at the magnetic footprint of the Polar satellite. Same meanings for (diamond, asterisk, and plus) data symbols and straight lines as in Figure 5a. The characteristic energies for H^+ and He^+ derived from all data samples (top panels) are believed to be significantly biased upward and are not reported here; see text.